基于小波包变换与自适应阈值的 SMT 焊点图像去噪

赵辉煌[1,2]，　周德俭[3]，　吴兆华[3]，　李春泉[3]，　李康满[1]

(1. 衡阳师范学院 计算机系，衡阳　421008；2. 西安电子科技大学 机电工程学院，西安　710071；
3. 桂林电子科技大学 机电工程学院，桂林　541004)

赵辉煌

摘　要：为提高表面组装技术焊点图像去噪效果，提出一种基于小波包变换和自适应阈值的焊点图像噪声去除新方法. 利用小波包变换对图像进行多层分解，通过对图像小波包树系数的分析，对小波包树系数高频部分和低频部分进行 Wiener 滤波；为提高去噪性能，通过计算小波包系数对应的中值绝对方差估计，提出一种改进的自适应小波包阈值算法，并对图像进行第二次去噪；最后采用中值滤波对图像进行平滑处理，得到最终的去噪图像. 结果表明，与传统方法相比，所提出的算法不仅能提高去噪性能和去噪效果，而且能很好的保留表面组装技术焊点图像边缘信息.

关键词：表面组装技术焊点；　图像去噪；　小波包变换；　自适应阈值

中图分类号：TG404　　**文献标识码**：A　　**文章编号**：0253－360X(2011)11－0073－04

0　序　　言

在表面组装技术(surface mount technology，SMT)焊点图像检测与识别研究中[1]，由于图像中存在不同性质的噪声，噪声降低了图像质量，使图像变得模糊，有时还会淹没图像的一些有效特征，给分析与研究带来困难. 由于 SMT 焊点中混合噪声存在，采用传统的方法去除 SMT 焊点图像去噪，去噪效果不是很理想，并且容易破坏图像的边缘信息. 在很多情况下，椒盐噪声与高斯噪声或乘性噪声同时存在 SMT 焊点图像中[2]. 小波包(wavelet packet)是小波概念的推广[3,4]，小波包分析能够为信号提供一种更加精细的分析方法，由于它不仅将低频带进行多层次划分，而且对多分辨分析没有细分的高频部分也进行进一步的分解. 因此小波包技术具有更广泛的应用价值，已被应用到模式识别、图像处理等许多领域[5,6]. Wiener 滤波器是一种经典的线性平滑滤波器，是基于最小均方误差原则而得到的一种局部自适应线性滤波器，它能够根据局部方差来调整输出. Wiener 滤波对已知噪声分布的噪声具有很好的去噪声特性[7]. 中值滤波(Median filter)是一种可以有效地抑制图像噪声，提高图像信噪比的非线性滤波技术，中值滤波器可以有效地滤除随机噪声和椒盐噪声，同时能够很好地保留图像的边缘细节. 为提高去噪性能，Wang[8] 提出小波包结合中值滤波算法(WPM)，在提高去噪性能上取得一定的效果.

文中对 SMT 焊点图像噪声去除方法进行研究，先对 SMT 焊点图像进行小波包分解，利用中值绝对方差估计方法估计原图像的噪声，结合 Wiener 滤波、改进自适应阈值和中值滤波(adaptive threshold of wavelet packet transform，wiener filter and median filter，AWPWM)，对图像进行去噪处理，同时保护边缘少受模糊.

1　基于小波包变换与自适应阈值的 SMT 焊点图像去除算法

1.1　小波包树系数据 Wiener 滤波

对 SMT 焊点图像进行小波包分解，图像被分解成高频、低频部分，图像噪声主要集中在高频部分，而图像有用信息主要集中在低频部分. 采用 Wiener 滤波，对小波包分解后的高频部分和部分低频部分进行滤波，有效去除图像中的混合噪声，同时较好地保留图像的边缘和高频细节信息. 对于不同层次的小波包分解，采用不同窗口大小的 Wiener 滤波，小波包系数 Wiener 滤波过程如图 1 所示.

1.2　自适应阈值去噪算法

传统的小波包阈值的方法是把图像系数保留，

收稿日期：2009－12－22
基金项目：广西省自然科学基金资助项目(0832242)

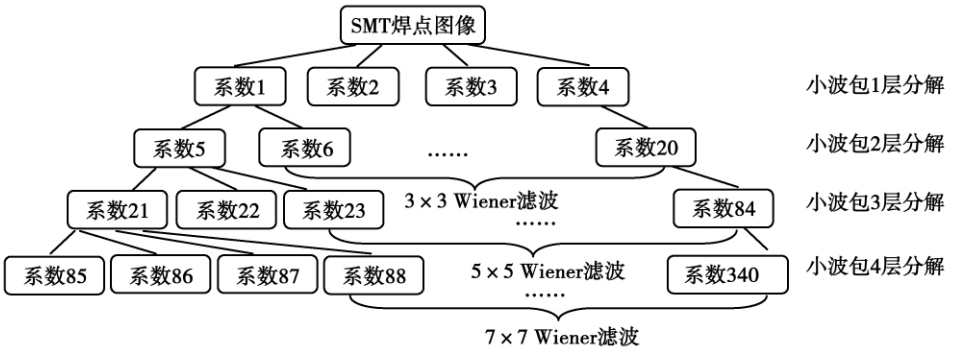

图 1 小波包树系数 Wiener 滤波

Fig. 1 Wavelet packet tree coefficients Wiener filtering

而把大部分噪声系数减少至零. 在实际应用中常见的阈值主要有 3 种, 分别为硬阈值、软阈值和半软阈值. 阈值选择得当与否直接影响去噪算法的有效性. 阈值选择过大,使得过多的小波包分解系数被置为零,破坏了过多的图像细节; 阈值过小,又不能达到预期的去噪效果[9,10]. 由于采用传统的阈值处理方法不能很好地达到去噪的要求,文中提出一种改进的基于自适应的阈值去噪方法,基本思想如下.

(1) 计算小波包 N 层分解的高频部分每一个小波包系数方差为

$$\sigma = \frac{\text{Median}(\ |w_{J,k}(s)|\ )}{0.674\ 5} \tag{1}$$

式中: J 为分解的层数; k 为小波包高频系数序列; Median( ) 为中值函数; $w_{J,k}(s)$ 为小波包系数; s 为噪声图像.

(2) 根据式(1)计算出的小波包系数对应的方差绝对值按从大到小降序排列.

(3) 根据步骤(2)得到的排列结果,得到排序后的中间值 $\sigma_{J,\mathrm{M}}$ 及对应的小波包系数 $w_{J,s}(m)$,$m = 1,2,3\cdots$; m 为小波包系数序列数.

(4) 根据步骤(1)得到的结果,按式(2)计算小波包树中高频系数 $w_{J,s}(s)$ 对应的最佳阈值在 $w_{J,d}(s)$ 中的位置 $P_{J,s}$,并得到最佳阈值 λ_s 为

$$P_{J,s} = N(s)^2 - \frac{J^J N(s)}{\sigma_{J,s}} \tag{2}$$

$$\lambda_s = |w_{J,s}(s)|_{P_{J,s}} \tag{3}$$

式中: $N(s)$ 为第 J 层分解后图像的宽度; J^J 为进行 J 层分解后的函数.

(5) 对小波包系数进行阈值处理得

$$w_{J,s} = \begin{cases} w_{J,s}, & |w_{J,s}| \geqslant \lambda_s \\ 0, & |w_{J,s}| \leqslant \lambda_s \end{cases} \tag{4}$$

$$w_{J,s} = \begin{cases} w_{J,s} - \lambda_s, & w_{J,s} \geqslant \lambda_s \\ 0, & |w_{J,s}| < \lambda_s \\ w_{J,s} + \lambda_s, & w_{J,s} \leqslant -\lambda_s \end{cases} \tag{5}$$

当 $s \leqslant m$ 时执行式(4), 当 $s > m$ 时执行式(5).

小波包高频系数进行最佳阈值处理后,得到新的小波包系数,重构图像. 图像经过二次去噪处理, SMT 焊点图像中的大部分噪声已经去除,但可能还存在有比较大的噪点无法去除,采用中值滤波平滑噪声,同时保护图像边缘信息,最终得到去噪图像.

2 基于小波包变换与自适应阈值的 SMT 焊点图像去噪算法流程

根据以上基于小波包变换与自适应阈值的图像噪声去除原理,设计 SMT 焊点图像噪声去除算法,流程如下.

(1) 选择小波包分解的最高层次 N,对 SMT 焊点图像进行小波包分解,得到各层的小波包系数.

(2) 利用 Wiener 滤波方法,对图像小波包树系数进行滤波处理.

(3) 计算小波包系数对应的方差绝对值,按从大到小降序排列,并得到中间值及对应的小波包系数.

(4) 根据上述改进自适应小波包阈值计算方法,计算出最佳阈值.

(5) 采用自适应阈值对小波包系数去噪,对图像进行第二次去噪处理.

(6) 重构小波包系数.

(7) 采用中值滤波对图像进行平滑处理,对图像进行第三次去噪处理,最终得到去噪后的 SMT 焊点图像. 算法流程如图 2 所示.

3 去噪性能比较

为比较其它方法与文中提出的方法的去噪性能,以最小均方误差(minimize the mean squared error, MSE) 作为比较参数,对含有椒盐噪声概率大小

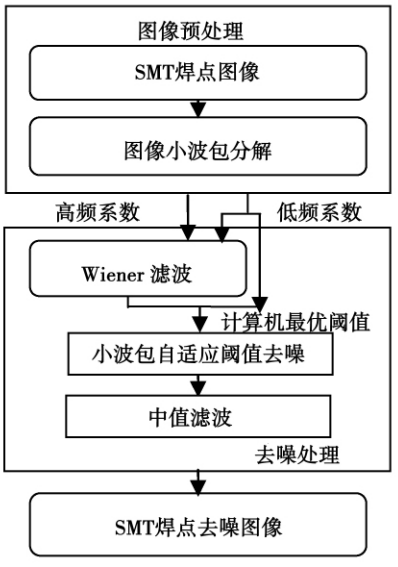

图 2　基于小波包变换与自适应阈值的 SMT 焊点图像去噪算法流程

Fig. 2　Process of SMT solder joint image denoising based on wavelet packet transform and adaptive threshold

0.02 和不同程度高斯噪声的“Lena”图像,采用不同去噪方法去噪得到相应最小均方差,并以此比较不同方法的去噪性能. 其中 Median 滤波和 Wiener 滤波采用窗口像素大小分别为 3 ×3,5 ×5,小波包变换分别采用 2,3,4 层分解. 文中只列出它们最佳去噪效果,计算得到 MSE 结果如表 1 所示.

表 1　几种方法的去噪性能比较

Table 1　Denoising performances of several methods

采用方法	最小均方误差(MSE) ε					
	$\sigma=15$	$\sigma=20$	$\sigma=25$	$\sigma=30$	$\sigma=35$	$\sigma=40$
Median	66.59	99.43	140.73	190.64	249.10	315.88
Wiener	177.08	184.30	194.37	207.69	224.83	246.11
WPM	96.64	103.30	111.33	120.62	131.17	142.75

由表 1 可以看出,在混合噪声强度比较弱的情况下,中值滤波能达到较好的去噪效果,但当混合噪声比较强的情况下小波包结合中值滤波(WPM) 的性能优于其它方法.

采用 AWPWM 方法,分别利用小波包 2 层分解, Wiener 窗口像素大小 3 ×3,中值滤波窗口像素大小 3 ×3(方法 1) ; 小波包 2 层分解,Wiener 窗口像素 5 ×5,中值滤波窗口像素 3 ×3(方法 2) ,小波包 3 层分解, Wiener 窗口像素 3 ×3,中值滤波窗口像素 5 ×5(方法 3) ; 和小波包 3 层分解, Wiener 窗口像素 5 ×5,中值滤波窗口像素 5 ×5(方法 4) ,结果如表 2 所示.

表 2　采用 AWPWM 方法图像混合噪声去除

Table 2　Denoising performances of AWPWM

采用方法	最小均方误差(MSE) ε					
	$\sigma=15$	$\sigma=20$	$\sigma=25$	$\sigma=30$	$\sigma=35$	$\sigma=40$
1	66.55	78.07	91.93	107.94	126.08	146.13
2	68.45	79.59	92.90	108.31	125.75	145.24
3	102.1	105.22	126.05	135.57	141.54	147.28
4	103.0	104.66	120.21	131.55	133.98	139.05

从表 2 与表 1 比较可得出,采用 AWPWM 方法得出的去噪方法,图像的 MSE 有较好的提高,该研究提出方法在混合噪声去噪性能上比其它传统几种方法都要好. 同时在新方法中,不同的混合噪声强度,采用不同的小波包层数分解和 Wiener 滤波窗口大小所获得的去噪性能也有所区别,这将在以后的工作中进行进一步研究.

4　SMT 焊点图像去噪结果及比较

乘性噪声也是在 SMT 焊点图像中常见的噪声之一,选取 IPC-A-610D 中翼型引脚焊点灰度图像为例, 如图 3a 所示. 添加椒盐噪声和乘性噪声如图 3b 所示.

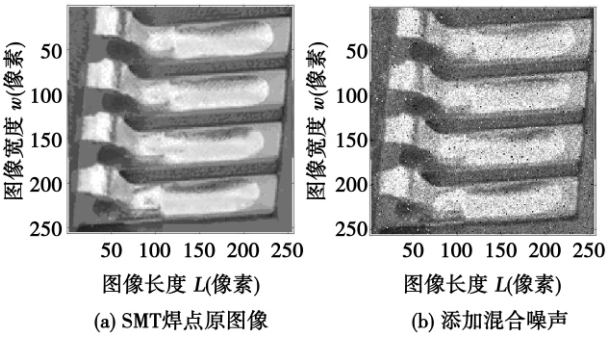

图 3　SMT 焊点图像及噪声图像

Fig. 3　SMT solder joint image and noised image

对于加噪图像,分别采用中值滤波(窗口像素大小 3 ×3) ,Wiener 滤波(窗口像素大小 3 ×3) ,小波包软阈值方法进行去噪,去噪结果分别如图 4 所示.

由图 4 可以得出, 中值滤波和 Wiener 滤波对 SMT 焊点图像的去噪效果不是很理想; WPM 方法去除较小的噪点有一定的效果,但对于大部分噪声,去除效果不是很好,仍被保留在图像中,采用文中提出的 AWPWM方法,中值滤波窗口像素大小分别为3

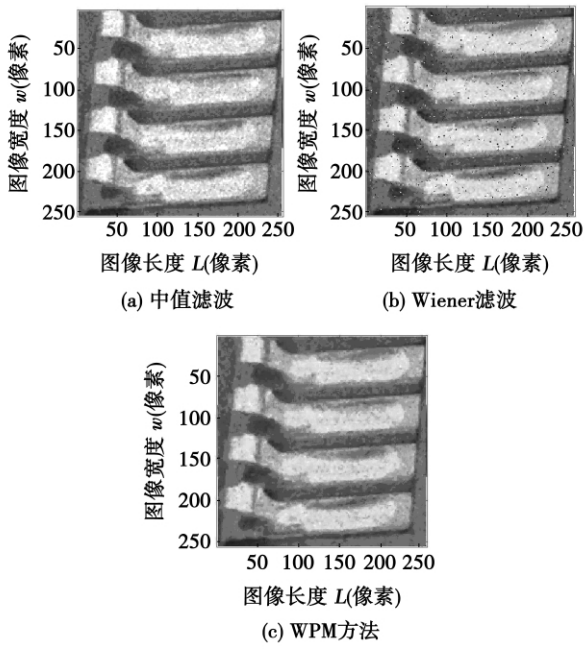

图 4 SMT 焊点图像去噪结果比较

Fig. 4 SMT solder joint image denoised results

×3,5×5,小波包变换分别采用 2,3 层分解. 结果如图 5 所示. 由图 5 与图 3b 比较可以得出,图 5 中焊点的噪点已基本消除,去噪目的达到,并且边缘信息保存良好. 去噪效果要优于图 4 所示的方法,且图 5b 的效果要略优于 5a 的效果.

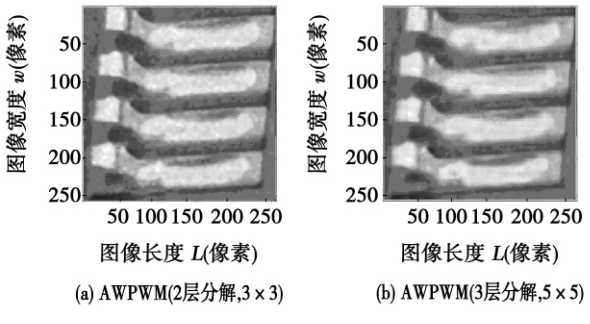

图 5 采用 AWPWM 方法 SMT 焊点图像去噪结果

Fig. 5 Image denoised result with AWPWM

5 结 论

(1) 采用 Wiener 滤波,对小波包分解后的高频部分和部分低频部分适当进行滤波,有利于提高 SMT 焊点图像去噪效果.

(2) 采用改进的自适应小波包阈值方法对小波包系数阈值处理,比传统的小波包阈值去噪思想更合理,能有效地去除 SMT 焊点图像中的混合噪声.

(3) 采用中值滤波对 SMT 焊点图像进行光滑处理,同时保护好图像的边缘信息.

参考文献:

[1] 周德俭, 黄春跃, 吴兆华, 等. 基于焊点虚拟成形技术的 SMT 焊点质量保证技术研究[J]. 计算机集成制造系统, 2006, 12(8): 1267 - 1272.
Zhou Dejian, Huang Chunyue, Wu Zhaohua, *et al*. SMT solder joints quality assurance based on solder joints virtual evolving technology [J]. Computer Integrated Manufacturing Systems, 2006, 12(8): 1267 - 1272.

[2] Kong Fanhui, Wang Yongxin. Reconstruction of solder joint surface based on shape from shading [C] // IEEE Third International Conference on Natural Computation, HaiNan, China, 2007: 58 - 62.

[3] Brechet L, Lucas M F, Doncarli C, *et al*. Compression of biomedical signals with mother wavelet optimization and best-Basis wavelet packet selection [J]. IEEE Transactions on Biomedical Engineering, 2007, 54(12): 2186 - 2192.

[4] 张文革, 刘 芳, 高新波, 等. 一种自适应多尺度积阈值的图像去噪算法[J]. 电子与信息学报, 2009, 31(8): 1779 - 1785.
Zhang Wenge, Liu Fang, Gao Xinbo, *et al*. An image denoising algorithm using adaptive multiscale products thresholding [J]. Journal of Electronics & Information Technology, 2009, 31(8): 1779 - 1785.

[5] Ercelebi E, Koc S. Lifting-based wavelet domain adaptive wiener filter for image enhancement [J]. IEEE Proceedings Vision, Image and Signal Processing, 2006, 153(1): 31 - 36.

[6] Silva J, Narayanan, Shrikanth S. Discriminative wavelet packet filter bank selection for pattern recognition [J]. IEEE Transactions on Signal Processing, 2009, 57(5): 1796 - 1810.

[7] Zha Xianjie, Fu Rongshan, Dai Zhiyang, *et al*. Noise reduction in interferograms using the wavelet packet transform and wiener filtering [J]. IEEE Geoscience and Remote Sensing Letters, 2008, 5(3): 404 - 408.

[8] Wang Huiyan. Noise reduction in pulse signal using the wavelet packet transform and median filtering [C] // 2008 International Workshop on Education Technology and Training & 2008 International Workshop on Geoscience and Remote Sensing, Shanghai, China, 2008: 675 - 679.

[9] Kopsinis Y, McLaughlin S. Development of EMD-based denoising methods inspired by wavelet thresholding [J]. IEEE Transactions on Signal Processing, 2009, 57(4): 1351 - 1362.

[10] Kingsbury M N. Image denoising using derotated complex wavelet coefficients [J]. IEEE Transactions on Image Processing, 2008, 17(9): 1500 - 1511.

作者简介: 赵辉煌,男,1982 出生,讲师,博士. 主要研究方向为制造自动化. 图像处理和模式识别. 发表论文 10 余篇. Email: zhaohuihuang278@163.com

The coated electrode had higher ability to prevent the electrode from plastic deformation during welding compared with the un-coated electrode. In addition, there were much more pitting, cracking, intermetallic alloy layer and self-healing layer on the end surface of un-coated electrode. As a barrier, the coatings on the surface of electrode could effectively prevent the adhesions, stripping, and then significantly reduce the diffusion of Zn from the surface of the electrode into the Cr-Zr-Cu electrode to form brittle intermetallic compounds.

Key words: Zn-coated sheet steel; resistant spot welding; coated electrode; metallic ceramic coating; electrode life

Control system for electron beam synchronous scanning based on CPLD PENG Yong[1], WANG Kehong[1], ZHOU Qi[1], WANG Yajun[2], FU Pengfei[3] (1. School of Materials Science and Engineering, Nanjing University of Science and Technology, Nanjing 210094, China; 2. School of Mechanical Engineering and Automation, Beijing University of Aeronautics and Astronautics, Beijing 100083, China; 3. National Key Laboratory of High Power Beam Processing Technology, Beijing Aeronautical Manufacturing Technology Research Institute, Beijing 100024, China). p 57 - 60

Abstract: For the quality diagnosis of electron beam in range from 5 mA to 60 mA of a high-voltage electron beam welding machine, a CPLD (Complex Programmable Logic Device)-based control system of electron beam high-speed scanning was established by means of analyzing the principle of electron beam scanning in the electromagnetic deflection coils. The control system consists of industrial PC, CPLD chip, DAC (Digital to Analog Convertor), low pass filter circuits, optical isolation circuits, power amplifiers, electromagnetic deflection coil and external circuits of CPLD. The system controls the special phase relationship between the two waveform and the trigger and sampling frequency of the acquisition card. The scanning frequency can be adjusted within the range 0 ~ 15.6 kHz. The amplified power is the constant current mode and its maximum output current is 5 A. The signal parameters can be adjusted to change the scanning path of electron beam without changing any hardware circuit, so it is highly flexible.

Key words: electron beam welding; CPLD; synchronous scanning; beam quality

Friction-stir welds (FSW) of spray formed 7475 aluminum alloy plate YAN Keng, SHI Chao (Provincial Key Lab of Advanced Welding Technology, Jiangsu University of Science and Technology, Zhenjiang 212003, China). p 61 - 64

Abstract: Friction-stir welds (FSW) of spray formed 7475 aluminum alloy plate with 4 mm thickness were studied. The shapes and dimensions of FSW tools as well as welding parameters were optimized based on mechanical tests and micro-analysis. Experimental results show that good-appearance welds can be achieved by optimal welding parameters. However, fin and groove defects appear if the welding parameters are not appropriate. It also shows that the mechanical properties of the joints are affected by the welding parameters. Some relations between the mechanical properties and the welding parameters were established. As the rotating speed is 1 200 r/min and the welding speed is 80 mm/min, the good weld is achieved and the tensile strength of the weld reaches 442 MPa.

Key words: spray formed 7475 aluminum alloy; FSW; technique; mechanical property

Influence of Ni on microstructure and processing performance of Ag-Cu-Sn-In brazing alloy XU Jinfeng[1], ZHANG Xiaocun[1], ZHAI Qiuya[1], DAI Weigang[2] (1. School of Materials Science and Engineering, Xi'an University of Technology, Xi'an 710048, China; 2. Changshu Shuanghua Electronic Co., Ltd., Changshu 215500, China). p 65 - 68

Abstract: Influence of Ni on the microstructure and processing performance of Ag-Cu-Sn-In brazing alloy was investigated. The microstructures of Ag-Cu-Sn-In of solder were composed of β-Cu coarse dendrite, (α-Ag) distributing in the interdendritic space and little Ag_5Sn. By adding Ni element, the grains refined, the melting point rised a little, and processability was influenced evidently. With Ni content increasing, rate of deformation is bigger, processability of brazing alloy is better. As Ni content was 0.2%, the rate of deformation reached maxinum. Ni content sequentially increasing, microstructures of brazing alloy are becoming bulkily, and processability is worse. With 0.2% Ni Content, the temperature of solidus and liquidus of alloy foils increased respectively by 18 ℃ and 8 ℃, the temperature interval decreased by 20 ℃. After annealing treatment, brazing alloy with 0.2% Ni can be rolled into foils of 50 ~ 80 μm thickness.

Key words: lower silver electrical vacuum brazing filler; melting point; microstructure; processability

Wettability and microstructure of Sn-Ag-Cu-In solder WANG Jianxin, YIN Ming, LAI Zhongmin, LI Xue (Province Key Lab of Advanced Welding Technology, Jiangsu University of Science and Technology, Zhenjiang 212003, China). p 69 - 72

Abstract: In order to improve the properties of Sn-1.2Ag-0.6Cu solder, small amount of In (0 ~ 1.0%) was added to the base alloys, the melting temperatures of alloys were tested, and the effect of In on the wettability and microstructure of solder alloy was studied. The melting temperature decreases with the addition of In. At the same soldering temperature, the lower melting temperature is, the higher superheat is, thus the viscosity of liquid solder is decreased and fluidity is improved. The zero time of Sn-1.2Ag-0.6Cu in air is below 1s at 260℃, while the zero time of Sn-1.2Ag-0.6Cu-1.0In in N_2 atomsphere is below 1s at 250℃, meeting the demand of IPC/EIA J-STD-003B. The Ag_3Sn in Sn-1.2Ag-0.6Cu alloy becomes coarser with 1.0% In added, which is harmful to the mechanical properties. Thenefore, the content of In addition into the Sn-1.2Ag-0.6Cu is not higher than 1.0%.

Key words: lead-free solder; wettability; microstructure

SMT soldering image denoising based on wavelet packet transform and adaptive threshold ZHAO Huihuang[1,2], ZHOU Dejian[3], WU Zhaohua[3], LI Chunquan[3], LI Kangman[1] (1. Department of Computer, Hengyang Normal University, HengYang 421008, China; 2. School of Mechano-Electronic Engineering, Xidian University, Xi'an 710071, China; 3. School of Mechanical and Electronical Engineering, Guilin University of

Electronic Technology, Guilin 541004, China). p 73 - 76

Abstract: A novel image processing approach is proposed to reduce the mixed noise in surface mount technology soldering image based on wavelet packet transformed adaptive threshold. At first, by using wavelet packet transform, the approach not only decomposes the image into the low frequency part but also into the high frequency part of image in several scales. After analyzing the wavelet packet tree coefficients, they were processed with the Wiener filter, and kept the wavelet packet tree low frequency coefficients without change. Secondly, an improved wavelet adaptive threshold algorithm is proposed to denoise the mixed noise again. At last, the inverse wavelet packet transform is applied to reconstruct the image and median filter is used to smooth the image. The experimental results have illustrated that the approach can obtain a better result in soldering image denoising compared with the conventional methods and can retain the image edges very well.

Key words: surface mount technology solder joint; image denoising; wavelet packet transform; adaptive threshold

Compared study on properties of SnZn-based lead free solders LAI Zhongmin[1], ZHANG Liang[2], WANG Jianxin[1] (1. School of Materials Science & Engineering, Jiangsu University of Science and Technology, Zhenjiang 212003, China; 2. School of Mechanical & Electrical Engineering, Xuzhou Normal University, Xuzhou 221116, China). p 77 - 80

Abstract: The wettability, creep resistance and mechanical properties of four SnZn-based solders were compared. Base on the wetting-balance test, the wettability of SnZnAg/SnZnGa/SnZnAl is better than SnZn solders. The addition of alloying elements can improve the wettability of SnZn alloys. With the testing of nanoindentation creep behavior of SnZn solders, it is found that the creep resistance of SnZnAg solder is highest of all, the mechanism is Ag-Zn particles acting as barriers to the motion of dislocations. In addition, with the testing of mechanical properties, the results show that the mechanical and thermal-fatigue resistance properties can be enhanced with the addition of alloying elements, the mechanical properties of SnZnAg solder joints is 20% higher than that of SnZn solder joints, the function of Ga/Al is less than Ag. Furthermore, using diode laser soldering, the mechanical properties of SnZn solder joints can increase up to 116.7%.

Key words: lead-free solders; creep resistance properties; intermetallic compounds; diode laser soldering

Pitting corrosion resistance of micro-zones in welded joint of 2205 duplex stainless steel BAO Yefeng[1], HU Wangqin[1], JIANG Yongfeng[1], YANG Ke[1,2] (1. Institute of Mechanical and Electronic Engineering, Hohai University, Changzhou 213022, China; 2. Advanced Welding Technology of Provincial Key Laboratory, Jiangsu University of Science and Technology, Zhenjiang 212003, China). p 81 - 84

Abstract: The microstructures of welded joint of 2205 duplex stainless steel were studied by optical microscope. Cyclic voltammetry curves of base material, weld metal and HAZ were measured by a self-designed micro electrochemical system respectively. The results show that the microstructures of welded joint of 2205 duplex stainless steel are ferrite and austenite. The percentage of ferrite in weld metal is about 48%, which is equivalent with that in base material, while the average ferrite content in HAZ is more than a half. In the 3.5% NaCl solution, the weld metal shows the consistent pitting corrosion resistance with the base material, but its repassivation behavior is not as good as the base material. Among the three micro-zones of the welded joint, HAZ shows the poorest pitting corrosion resistance and repassivation behavior. The differences on pitting corrosion resistance of different micro-zones of welded joint are relevant to the phase ratio and the distribution of alloy elements in phases.

Key words: duplex stainless steel; microstructure; micro-electrochemical method; pitting corrosion

Impact toughness of simulated CGHAZ with high heat input for adding trace Zr oil tank steel LIANG Guoli[1,2,3], YANG Shanwu[1], WU Huibin[2], LIU Xueli[2] (1. Department of Material Physics and Chemistry, University of Science Technology of Beijing, Beijing 100083, China; 2. National Engineering Research Center for Advanced Rolling Technology, University of Science Technology of Beijing, Beijing 100083, China; 3. Department of Electro-Mechanical Engineering, Tangshan College, Tangshan 063000, China). p 85 - 88

Abstract: The effects of trace Zr element on impact toughness of coarse grain heat affected zone (CGHAZ) of 690 MPa grade oil tank steel was investingated with the high heat-input welding cycle using Gleeble3500. The results showed that trace Zr treated steel can significantly improve low temperature impact toughness of base metal, but it could seriously worsen the impact toughness of CGHAZ. The M-A component of trace Zr treated steel coarsed with the heat input increasing, the area percentage of M-A component decreased with the heat input increasing, which resulted in the steel toughness decreasing. The size of inclusions containing Zr are all micron level, and were precipitated in the solidification process, which have litte effect on strenghen and grain refinement, but has a very important influence on impact toughness. The oversize inclusions (1-3 μm) could result in the impact toughness decreasing.

Key words: oil tank steel adding trace Zr; high heat-input welding; CGHAZ; impact toughness

Sensitivity analysis and prediction of double ellipsoid heat source parameters LI Peilin, LU Hao (School of Material Science and Engineering, Shanghai Jiao Tong University, Shanghai 200240, China). p 89 - 91, 95

Abstract: When the arc force is strong, the double ellipsoid heat source model is the most widely used heat source model. The influence of the heat source parameters on the weld size was researched, and the sensitivity of the double ellipsoid heat source parameters was obtained for SAW. The multiple regression analysis was applied to research the relationship between the weld size and the heat source parameters. An empirical formula was put forward, and the heat source parameters corresponding to the weld width and penetration can be easily calculated by the empirical formula. The trial time is reduced and the simulation precision is increased.

Key words: submerged arc welding; double ellipsoid